BACHELOR'S THESIS

Degree in Mathematics

Title: Computational Modeling of Single Cell Migration

Author: Daniel Araya Matilla

Advisor: Pablo Sáez Viñas

Department: Mathematics

Academic year: 2020-2021

UNIVERSITAT POLITÈCNICA DE CATALUNYA
BARCELONATECH
Facultat de Matemàtiques i Estadística

UNIVERSITAT POLITÈCNICA DE CATALUNYA
BARCELONATECH
Facultat de Matemàtiques i Estadística

Degree in Mathematics
Bachelor's Degree Thesis

Computational Modeling of Single Cell Migration

Daniel Araya Matilla

Supervised by Pablo Sáez Viñas

September, 2021

Acknowledgements

I would like to thank my supervisor Pablo for initiating me in this field, for showing me what research is and the huge help he has given. Thanks to my family for being always supportive and the trust they put in me.

Contents

1 Introduction

1.1 Cell migration

Cells are the basic biological structure of all organisms and their behavior has been and still is a key field of study in biology. A crucial property of cells is their ability to move, which is fundamental in many vital processes like wound healing, immune responses and cancers metastasis [1]. Cell migration takes two major features: determination of the direction in which to move and the movement itself. The process where the cell is not stationary anyomore and its symmetry is broken toward a specific direction is called polarization. [2]

Once the cell has a well-defined front and rear, it crawls on the surface by using a simple mechanical cycle consisting on protrusion, adhesion and contraction. Actually, these steps take place continuously and simultaneously, so they can be studied all at once [3]. For the protrusion, cells use flat motile appendages called lamellipodia. These appendages are made of actin filaments (F-actin), enveloped by the cell membrane, that grows because of the polymerization of actin monomers (G-actin). The latter diffuses in the cytoplasm and assembles onto uncapped filament barbed ends, at the leading edge. Actin polymers crosslink and generates a meshwork, which has been characterized as a complex viscous gel. Adhesion complexes, comprised of a protein called integrin, remain the cell attached to the substrate. Finally, lamellipodial contraction is mainly caused by myosin motors. Myosin molecules are distributed throughout the cell and each one develops a pN-range force [4]. This process does not disturb the stiff actin network in the front half of the lamellipod but actin chains disassembles backwards generating a retrograde flow inside the cell. This organization of the actin-myosin network, as well as the adhesion system, is the responsible for the movements and forces of the motile cell. It has been shown experimentally in [5] that lamellipodia fragments are able to move without a nucleus, this is why it makes sense to focus just on this components and not in the cell body.

Commonly, before the cell crawls by itself via the actin-myosin continuous cycle, it needs an external cue for the cell to polarize. Among all the ways to orientate a cell, here we see two that have been well studied before. On the one hand, we know some proteins of the Rho family like GTPases stimulate actin polymerization. Both active GTPases in the membrane and cytosolic inactive GTPases work as a closed system via activation/inactivation. Then, active forms

might increase their concentration on one side, which will be the front side of the cell [6]. Secondly, we know that friction gradients on the extracellular matrix do stimulate cell movement, what has been well studied in [2]. The cell moving because of a chemical cues we call it chemotaxis, while if the movement occurs due to a stiffness gradient on the substrate it is known as durotaxis.

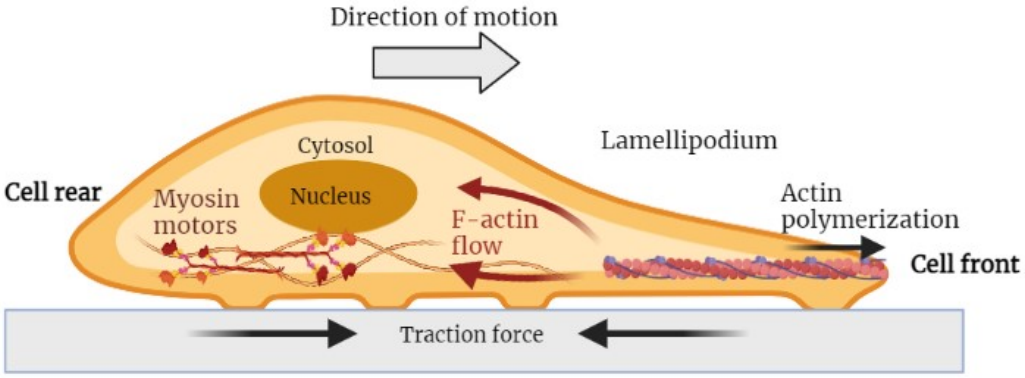

Figure 1.1: Schematic of the motile cell. There is already a well defined leading and rear edge. Lamellipodium grows in the front because of actin polymerization. Actin network disassembles backwards, which induce a retrograde flow. Myosin motors generate contractile stress on the actin meshwork and traction force due to cell attachments.

1.2 Mathematical modelling of cell migration

Cell motility has been well investigated and has a very rich experimental data. It is also safe to say that most of molecular parts underlying cell migration are known. Thus, numerous mathematical models have been proposed to replicate experimental results in order to understand and reproduce this process. Although mathematical models do not work directly with biological objects in the lab, they are essential since they are highly reliable and allow us to describe complex systems. Computational simulations also helps to carry out expensive experiments with low-cost tools and they provide new insights in cell motility.

Most of the cell migration models are built using several physical laws. The fundamental ones are the force balance principle and the conservation of mass. Moreover, all this occurs in such small space that inertia is negligible. We can differentiate two kind of forces. Active ones, which consume energy via ATP hydrolysis, like actin polymerization or myosin contractile stress. And passive ones, which conserve or dissipate energy, like friction or membrane tension. Conservation of mass states that the number of molecules can change owing only to transport (convection or diffusion) or chemical processes. These principles are used in most of models. However, constitutive relations, which are additional assumptions that

complement previous laws, must be discussed explicitly. For example, some models like the one in [3] do not consider actin meshwork as a viscous gel strip, but as viscoelastic or actin transport is driven just by convection and it does not diffuse in [4]. Actin polymerization velocity is also open to different descriptions in order to give the best approximation: while some consider that it evolves as function of the cell length like $\sim 1/x$ [3], others think that it develops like $\sim exp(-x)$ [7].

Regarding to initial polarization, a challenge is to know which specific polarization mechanism or combination of mechanisms works in every specific system. Together with lab work, modelling remains relevant to comprehend this problem. Another question that nowadays is still asked is whether motility starts by polarizing the cell front via protruding appendages or by defining first the rear and then allowing protrusion in the opposite side. In [8] they refer to mathematical models where actin flow accelerate in the future rear edge, and only then the opposite edge starts to enlarge. They justify this by saying that inward actin flow in one edge bundle the gel and result in a membrane tension drop, which allow the protrusion of the other edge. In fact, recent experiments confirmed that membrane tension is a crucial regulator of cell polarization [11]. Here we expect a similar behaviour of the cell when actin flow increase due to friction gradients and we combine it with external-signaling cues of GTPases proteins.

We develop here a one-dimensional model of the cell. This kind of representations are less accurate than two-dimensional ones because they do not reproduce the correct shape of the cell. However, 1D models are also useful since they are computationally less expensive, so we can execute simulations multiple times and with different purposes. Our objective is to develop a model that includes essential components of motility such as the velocity and stress of the actin meshwork, myosin-based contraction of the gel or the implementation of different kind of polarization mechanisms.

2 Mathematical framework

2.1 Actin mechanics

Actin mechanics involve the physics of a fluid in motion. The forces on the cell are the internal active and passive stress, and the friction force due to the contact with the substrate. Let σ be the total gel's stress. Then, the force-balance equation of F-actin is

$$\frac{\partial \sigma}{\partial x} = \eta v \tag{2.1}$$

where the right hand-side of the equation describes the interaction of the cell with the extracellular matrix and η is the friction coefficient. All the model parameters are listed in Table 1. We describe the actin network as a purely viscous gel. Thus, the total stress σ is the sum of active stress, due to actin-myosin interaction and passive stress generated by the viscosity. Then, σ can be written as

$$\sigma = \mu \frac{\partial v}{\partial x} + \xi \rho_a \rho_m \tag{2.2}$$

where the first term refers to the viscous stress, being μ the viscosity coefficient and the second term is the active stress produced by the contractile forces. ρ_a and ρ_m are the actin and myosin densities respectively and ξ is the contractility constant. Substituting the expression for the stress we have the extended momentum balance equation

$$\frac{\partial}{\partial x}\left(\mu \frac{\partial v}{\partial x} + \xi \rho_a \rho_m\right) = \eta v \tag{2.3}$$

To complete the formulation we need to specify the boundary conditions of the equation. We impose the tension at the leading and rear edge and we call this the membrane tension σ_m, which depends on the membrane extension. In the expansion phase of spreading, the cell length increases rapidly until it reaches a steady state length. Actually, the membrane has initially many folds that flatten during spreading and they let the cell to grow freely. During this process, the membrane does not restrain cell growth so we consider $\sigma_m = 0$. However, when all membrane folds deplete, this is, when cell length have grown about a 50% [9] of the initial length, we will calculate the membrane tension as $\sigma_m = \kappa(L - L_0)$. κ is a constant parameter and L_0 the initial cell length when all folds deplete. We consider σ_m an outward tension without regard of the cell direction, so it follows

that

$$\left(\mu\frac{\partial v}{\partial x}+\xi\rho_a\rho_m\right)\Bigg|_{\text{left edge}}=-\sigma_m \tag{2.4}$$

$$\left(\mu\frac{\partial v}{\partial x}+\xi\rho_a\rho_m\right)\Bigg|_{\text{right edge}}=\sigma_m \tag{2.5}$$

2.2 Transport mechanisms in cell migration

It is important to note that the previous mechanical variables change with position depending on the density of the actin network. We describe the actin and myosin density as a function of the position x and the time t and we will see that the motion of both densities are affected by the velocity v. However, while v is calculated in the lab frame of reference, the actin and myosin density movement depend only on the action inside the cell, i.e. the cell frame.

To find the velocity of the gel at each position in the cell frame, we use the classical velocity addition

$$v(x)=\tilde{v}(x)+v_{cell}(x) \tag{2.6}$$

This is, at each x, the velocity of the actin network in the lab frame v is the velocity in the cell frame $\tilde{v}$ plus the velocity of the cell v_{cell}. The velocity of the cell at each position is computed assuming that $v_{cell}=v+v^p$ (v^p is the protrusion velocity computed in equation 2.17) in the leading and rear edge and interpolating linearly along the length. Finally, we can calculate the velocity of the whole cell by computing the average between v_{cell} at the leading and rear edge.

2.2.1 Actin

We describe the conservation law for the actin density $\rho_a(x,t)$ as the motion equation for a physical quantity in a velocity field. In this particular case, considering the one dimension equation we have the following transient convection-diffusion-reaction equation

$$\frac{\partial\rho_a}{\partial t}+\frac{\partial}{\partial x}\left(\tilde{v}\rho-D_a\frac{\partial\rho_a}{\partial x}\right)=k_p-k_d\rho_a \tag{2.7}$$

where the source term involves k_p and k_d, this is, the polymerization and depolymerization rate respectively and D_a is the diffusive parameter. Note that depolymerization depends on the density, while polymerization depends only on the actin monomers, which is constant. The boundary conditions of the transport problem are essentially no flux boundary conditions. This means that there is no actin crossing the cell boundary. The BC equation reads

$$\tilde{v}\rho_a-D_a\frac{\partial\rho_a}{\partial x}=0 \quad \text{on} \quad \partial\Omega \tag{2.8}$$

We can decide which initial condition we state for ρ according to each need. Here we work with a small random generated profile centered on one since actin density is assumed to be distributed uniformly along the cell.

$$\rho_a(x,0) = \frac{\rho_0}{\overline{\rho_0}}, \qquad \rho_0(x) = 1 + 0.105\left(\frac{U(0,1)(x)}{2} - 1\right) \tag{2.9}$$

being $U(0,1)$ the uniform distribution in the $(0,1)$ interval.

2.2.2 Myosin

We develop our model where the internal flow is generated in part by myosin motors. They can stretch or squeeze the actin network in order to generate a mechanical stress and induce movement. To model the myosin distribution, we assume that they may be either bound or unbound to F-actin meshwork. Despite myosin motors attach and detach F-actin, total amount of mass is conserved. Thus, we follow the procedure done in [10] by combining both equations for bound and unbound myosin concentration into one single transport equation.

$$\frac{\partial \rho_m}{\partial t} + \frac{\partial}{\partial x}\left(\tilde{v}\rho_m - D_m\frac{\partial \rho_m}{\partial x}\right) = 0 \tag{2.10}$$

We impose boundary conditions to ensure no concentration of myosin go across the edges.

$$\tilde{v}\rho_m - D_m\frac{\partial \rho_m}{\partial x} = 0 \quad \text{on} \quad \partial\Omega$$

2.3 Polarization of signaling cues

In early events of migration, the cell can receive external signals in order to orientate it towards the proper direction. To achieve a polarized state, they are subjected to transient stimulus in the form of a shallow chemical gradient or a strongly localized signal on the cell membrane. The cell then responds by reorganizing into two well-defined regions, the front and the back edge. This all has well studied in [6].

There are many proteins involved in this process, like members of Rho GTPasas family such as Cdc42, Rac and Rho. They can be found in most of living being and they play a central role in cell motility. In our model we consider a simplified system compounded just of GTPasas because it helps to cover the essential features, although other proteins could be candidates for similar phenomena. Every Rho GTPasa cycle between the plasma membrane in a active form and cytoplasm as inactive forms. Actually, rates of transition and relative diffusion rates are known from experimental data. Here we followed a model for the signaling polarization called wave-pinning. The idea of the model relies on two reaction diffusion PDEs

with bistable kinetics, namely, propagation of fronts. We also considered a positive feedback from the activation form on its own production via GEFs (Guanine nucleotide Exchange Factors). On the other hand, the conversion from active to inactive forms is considered constant. Both equations, for active GTPase density R and inactive forms R_i are

$$\begin{cases} \dfrac{\partial R}{\partial t} - D_R \dfrac{\partial^2 R}{\partial x^2} = k_{on} R_i - k_{off} R & (2.11) \\ \dfrac{\partial R_i}{\partial t} - D_{R_i} \dfrac{\partial^2 R_i}{\partial x^2} = k_{off} R - k_{on} R_i & (2.12) \end{cases}$$

where k_{on} and k_{off} are the activation and inactivation rates respectively. The diffusion rate of the membrane-bound (active) form is known to be significantly smaller than the inactive one, so that $D_R \ll D_{R_i}$. Bistabilty requires that one of activation or inactivation rates (or both) be nonlinear. Here we have chosen one of the simplest assumption, this is a positive feedback from the activated forms, whereas the reverse conversion takes place constant. The expressions are

$$k_{on} = k_0 + \frac{\gamma R^2}{K^2 + R^2}, \qquad k_{off} = 1 \tag{2.13}$$

where $k_0 = 1s^{-1}$ is a basal GEF conversion rate, $\gamma = 1$ the maximal rate and $K = 1$ the saturation parameter.

Moreover, an external stimulus is known to increase activation of proteins by upregulating the GEFs that convert inactive forms to active forms. To model this external stimulus, we added a function $f_S(R_i)$ to equation 2.8 and subtracted from equation 2.9. We note it as

$$f_S = k_S(x,t) R_i \tag{2.14}$$

where $k_S(x,t)$ is the increased rate of conversion from inactive to active forms due to an external signal. We define k_S as a graded linear stimulus focused on one side

$$k_S = s(t)(L - x) \qquad x \in [0, L] \tag{2.15}$$

with

$$s(t) = \begin{cases} S_0 & 0 \le t \le t_1 \\ S_0 \left(1 - \dfrac{t - t_1}{t_2 - t_1}\right) & t_1 \le t \le t_2 \\ 0 & \text{otherwise} \end{cases} \tag{2.16}$$

where $S_0 = 0.07$ and t_1,t_2 are the points in time at which the stimulus starts to decrease and is finally null [6].

2.4 Protrusion velocity balanced by signaling cues and membrane tension

Next, we model the velocity of lamellipodial protrusion, which is driven by actin polymerization that pushes the plasma membrane forward. The cell membrane

is the leading structure to be pushed forward so it is reasonable to think that it also exerts an opposite force against the actin polymerization. This force is the membrane tension and it has been characterize experimentally and theoretically in the past together with its relation to actin polymerization describing force-velocity relations [11].

When there is no opposing forces to actin polymerization, some models like the one developed by Mogilner and Oster in [12] considered a free growth of the cell front with velocity $v_0^p = k_p \delta \rho^s$. Here k_{on} is the rate of actin assembly at the front, ρ^s is the density of polymerizable factors, that promotes or inhibit actin polymerization, and δ is the size of one single monomer at the tip of the filament. The free velocity is $v_0^p = 0.55 \mu$m/s [7]. However, the tension of the plasma membrane imposes a resistance to actin polymerization. Then, the actual protrusion velocity decreases with respect to the free polymerization velocity as

$$v^p = v_0^p exp(-\sigma_m \delta / k_B T) - \delta k_d \tag{2.17}$$

where σ_m is the resistance tension of the cell membrane per unit length and $k_B T$ is the thermal energy constant [7].

Moreover, in our model we do not consider v_0^p as a constant, but we impose it as a function of active GTPases concentration R. We formulated the function according to the following assumptions: there is no velocity when R tends to zero so $v_0^p(0) \approx 0$. When $R = 1$, which actually may be a real initial condition, we impose a free velocity $v_0^p(1) = 0.55$ and when $R \gg 1$ we impose a maximum velocity $v_0^p(R_{\max}) = 1.1$. Finally, the function we thought best fitted the demands was a sigmoid

$$v_0^p(R) = \frac{1.1}{1 + e^{-10(R-1)}} \tag{2.18}$$

Table 1: Model parameters

Parameter	Definition	Typical value	References
μ	Viscous coefficient	30 kPa s μm^{-2}	[12]
ξ	Contractility	0.015 kPa	[10]
η	Friction	3 kPa s	[10]
κ	Membrane stiffness	0.5 kPa μm^{-1}	[10]
k_p	Polymerization rate	0.1 s^{-1}	[15]
k_d	Depolymerization rate	0.1 s^{-1}	[15]
D_a	Actin diffusion coefficient	0.3 μm^2 s^{-1}	[12]
D_m	Myosin diffusion coefficient	0.7 μm^2 s^{-1}	[12]
k_{off}	GTPases inactivation rate	1 s^{-1}	[6]
D_R	Active GTPases diffusion coefficient	0.1 μm^2 s^{-1}	[6]
D_{R_i}	Inactive GTPases diffusion coefficient	10 μm^2 s^{-1}	[6]

2.5 Finite element implementation

We solved the model equations by using a finite element scheme for the spatial derivatives and a θ-method for the time integration when needed. Let us see how we get the numerical scheme for each equation.

2.5.1 Momentum-balance

Let us consider the main equation for the actin mechanics

$$\frac{\partial}{\partial x}\left(\mu\frac{\partial v}{\partial x}+\xi\rho_a\rho_m\right)=\eta v \tag{2.19}$$

Recall we noted as μ the viscous coefficient, ξ the contractibility constant and η the friction parameter. To approximate a solution with the finite element method we must state first the weak form of the problem, so we consider a proper Hilbert space $V \subset H^1(\Omega)$. Then, we multiply the whole equation by a test function $w \in V$ and integrate in Ω.

$$\int_\Omega w(\mu v_x+\xi\rho_a\rho_m)_x\,dx=\int_\Omega \eta w v\,dx$$

If we apply integration by parts in the left side we get

$$-\int_\Omega \mu w_x v_x\,dx-\int_\Omega \xi w_x\rho_a\rho_m\,dx+w\sigma\Big|_{\partial\Omega}=\int_\Omega \eta w v\,dx$$

We used $\mu v_x+\xi\rho_a\rho_m=\sigma$ and, since in the middle integral it is evaluated on the edges of the cell, we will note it as the membrane tension σ_m. Rearranging terms we obtain the weak form of the problem: find $v \in V$ such that

$$-\int_\Omega \mu w_x v_x\,dx-\int_\Omega \eta w v\,dx=\int_\Omega \xi w_x\rho_a\rho_m\,dx-w\sigma_m \qquad \forall w\in V \tag{2.20}$$

For the discretization, let us set $\Omega=[0,L]$ and a partition of the interval given by $X=[x_0,...,x_N]$ having $x_0=0$ and $x_N=L$. Furthermore, we define the space $V^h \subset V$ with $\dim V^h=|X|$ and a basis $\{N_i\}$ such that $N_i(x_j)=\delta_{ij}$. Thus, the approximate problem is now to find $v^h \in V^h$ saitsfying the weak form for all $w \in V^h$. In fact, it suffices that equation 2.17 be verified for each function of the basis, as they generate V^h. In this discrete space, functions v is approximated as

$$v^h=\sum_{j=0}^{N} N_j(x)v_j \tag{2.21}$$

Substituting in the weak form, we get

$$-\mu\sum_j\left(\int_\Omega N_i'N_j'\,dx\right)v_j-\eta\sum_j\left(\int_\Omega N_iN_j\right)v_j=\int_\Omega \xi N_i'\rho_a\rho_m\,dx-N_0\sigma_m+N_N\sigma_m$$

for all $i = 0, ..., N$. Finally, just can write the whole system of N equations as a matricial algebraic equation

$$(-\mu \mathbf{K_v} - \eta \mathbf{K_f})\, \boldsymbol{v} = \mathbf{f} \tag{2.22}$$

where

$$\mathbf{K_v} = \int_\Omega N_i' N_j'\, dx \qquad \mathbf{K_f} = \int_\Omega N_i N_j\, dx \qquad \mathbf{f} = \int_\Omega \xi N_i' \rho_a \rho_m\, dx - N_0 \sigma_m + N_N \sigma_m$$

Once the system is solved, we will have found the velocity $v(x)$ of the cell gel in the lab frame. Hence, before solving transport equations, we must change the frame of reference where velocity v is into a cell-frame velocity $\tilde{v}$. This is done by using the classic addition $v_{cell} + \tilde{v} = v$.

2.5.2 Transport equation

We consider now the transport problem for actin and myosin densities. The numerical approximation can be solved in general since both problems are transient convection diffusion PDEs. Here we use the equation for the actin density but the procedure and final system is analogous for myosin concentration ρ_m (we just would consider no source term). Recall the equations of actin transport

$$\begin{cases} \dfrac{\partial \rho_a}{\partial t} + \dfrac{\partial}{\partial x}\left(\tilde{v}\rho_a - D_a \dfrac{\rho_a}{\partial x}\right) = k_p - k_d \rho_a & (x,t) \in \Omega \times [0,T] \\ \tilde{v}\rho_a - D_a \dfrac{\partial \rho_a}{\partial x} = 0 & \text{on } \partial\Omega \end{cases} \tag{2.23}$$

The same method as in the mechanics equation for the actin motion is used so we take a proper Hilbert space V and $w \in V$. We multiply the whole equation by w ans integrate in the domain Ω

$$\int_\Omega w \partial_t \rho_a + \int_\Omega \partial_x(\tilde{v}\rho_a - D_a \partial_x \rho_a)\, w = \int_\Omega k_p w - k_d \rho_a w$$

applying integration by parts in the second expression we get

$$\int_\Omega w \partial_t \rho_a + \int_{\partial\Omega} (\tilde{v}\rho_a - D_a \partial_x \rho_a) w - \int_\Omega (\tilde{v}\rho_a - D_a \partial_x \rho_a) \partial_x w = \int_\Omega k_p w - k_d \rho_a w$$

Since we have no-flux boundary conditions on the front and rear edge, the integral on $\partial\Omega$ is null. Thus, the weak formulation of the problem is: find a ρ_a in V such that

$$\int_\Omega w \partial_t \rho_a - \int_\Omega \tilde{v}\rho_a \partial_x w + \int_\Omega D_a \partial_x \rho_a \partial_x w + \int_\Omega k_d \rho_a w = \int_\Omega k_p w \qquad \forall w \in V \tag{2.24}$$

We discretize the problem in the same space V^h where we solved the momentum-balance equation. Therefore, using the discrete approximation $\rho_a = \sum N_j(x)\rho_{aj}$ we can write the equation as

$$\sum_{j=0}^{n}\left(\int_\Omega N_i N_j\,dx\right)\dot{\rho}_{aj} - \sum_{j=0}^{n}\left(\int_\Omega \tilde{v}N_i' N_j\,dx\right)\rho_{aj} + D_a\sum_{j=0}^{n}\left(\int_\Omega N_i' N_j'\,dx\right)\rho_{aj} + k_d\sum_{j=0}^{N}\left(\int_\Omega N_i N_j\,dx\right)\rho_{aj} = \int_\Omega k_p N_i\,dx \tag{2.25}$$

for all $i = 0, ..., N$. The system of ODEs can be stated as an algebraic matricial equation

$$\mathbf{M}\dot{\boldsymbol{\rho}}_a + (D_a\mathbf{K} - \mathbf{C} + k_d\mathbf{M})\boldsymbol{\rho}_a = \mathbf{f}$$

where each matrix and the right hand side vector are computed as

$$\mathbf{M} = \int_\Omega N_i N_j\,dx \quad \mathbf{C} = \int_\Omega \tilde{v}N_i' N_j\,dx \quad \mathbf{K} = \int_\Omega N_i' N_j'\,dx \quad \mathbf{f} = \int_\Omega k_p N_i\,dx$$

for $i, j = 0, ..., N$.

The time integration is given by the so called θ-method. The latter discretizes the temporal derivative by a simple incremental ratio and replaces the other terms via a linear combination of ρ at time n and $n+1$, depending on the real parameter θ, with $0 \leq \theta \leq 1$. The idea is, given a first order ODE $y' = f(x, y)$, we approximate it as $\frac{Y^{n+1}-Y^n}{\Delta t} = \theta f(x^n, Y^n) + (1-\theta)f(x^{n+1}, Y^{n+1})$. We use this scheme because its ease to change the method by varying θ. Note that for $\theta = 1$ it is the explicit Euler, if $\theta = 0$ it is implicit Euler and if $\theta = 1/2$ we have Crank-Nicolson. In the whole work we use $\theta = 1/2$ (Crank-Nicolson method) since it is an implicit and second order method.

In our equation we have

$$\mathbf{M}\frac{\boldsymbol{\rho}_a^{n+1} - \boldsymbol{\rho}_a^n}{\Delta t} + (D_a\mathbf{K} - \mathbf{C} + k_d\mathbf{M})(\theta\boldsymbol{\rho}_a^{n+1} + (1-\theta)\boldsymbol{\rho}_a^n) = \theta\mathbf{f}^{n+1} + (1-\theta)\mathbf{f}^n$$

Note that in our particular case, $\mathbf{f}$ is constant in time, i.e $\mathbf{f}^n = \mathbf{f}$ for all n. Thus, $\theta\mathbf{f}^{n+1} + (1-\theta)\mathbf{f}^n = \mathbf{f}$. Then, the final system to be solved has the form

$$\left[\frac{\mathbf{M}}{\Delta t} + \theta(D_a\mathbf{K} - \mathbf{C} + k_d\mathbf{M})\right]\boldsymbol{\rho}_a^{n+1} = \left[\frac{\mathbf{M}}{\Delta t} + (1-\theta)(D_a\mathbf{K} - \mathbf{C} + k_d\mathbf{M})\right]\boldsymbol{\rho}_a^n + \mathbf{f} \tag{2.26}$$

2.5.3 Signaling equations

The last PDEs we need to solve numerically are the equations for both active and inactive GTPases densities together with the external stimulus k_s

$$\begin{cases} \dfrac{\partial R}{\partial t} - D_R \dfrac{\partial^2 R}{\partial x^2} = k_{on} R_i - k_{off} R + k_s R_i \\ \dfrac{\partial R_i}{\partial t} - D_{R_i} \dfrac{\partial^2 R_i}{\partial x^2} = k_{off} R - k_{on} R_i - k_s R_i \end{cases} \tag{2.27}$$

In order to solve this system we implemented, as before, a finite elements discretization in space and Crank-Nicolson method for the time integration. After the time discretization we get

$$\frac{\Delta R}{\Delta t} = \theta R_t^{n+1} + (1-\theta) R_t^n \tag{2.28}$$

$$\frac{\Delta R_i}{\Delta t} = \theta R_{it}^{n+1} + (1-\theta) R_{it}^n \tag{2.29}$$

where $\Delta(\cdot) = (\cdot)^{n+1} - (\cdot)^n$. Then, if we carry out the weak form and discretize it in the space we end up having the following system

$$\begin{aligned} \mathbf{M}\frac{R^{n+1} - R^n}{\Delta t} = \theta &\left[D_R \mathbf{K} R^{n+1} + \int N_i k_{on} R_i^{n+1}\, dx - k_{off}\mathbf{M} R^{n+1} + \int N_i k_s R_i^{n+1}\, dx \right] \\ &+ (1-\theta)\left[D_R \mathbf{K} R^{n} + \int N_i k_{on} R_i^{n}\, dx - k_{off}\mathbf{M} R^{n} + \int N_i k_s R_i^{n}\, dx \right] \end{aligned} \tag{2.30}$$

$$\begin{aligned} \mathbf{M}\frac{R_i^{n+1} - R_i^n}{\Delta t} = \theta &\left[D_{R_i} \mathbf{K} R_i^{n+1} - \int N_i k_{on} R_i^{n+1}\, dx + k_{off}\mathbf{M} R^{n+1} - \int N_i k_s R_i^{n+1}\, dx \right] \\ &+ (1-\theta)\left[D_{R_i} \mathbf{K} R_i^{n} - \int N_i k_{on} R_i^{n}\, dx + k_{off}\mathbf{M} R^{n} - \int N_i k_s R_i^{n}\, dx \right] \end{aligned} \tag{2.31}$$

with

$$\mathbf{M} = \int_\Omega N_i N_j\, dx \qquad \mathbf{K} = \int_\Omega N_i' N_j'\, dx$$

When solving the coupled system, we note that it is non-linear because of the term k_{on} (defined in equation 2.13). Therefore, we need to solve it iteratively using a fixed point method. First, using the equations we need to solve, we define the residuals

$$\begin{aligned} \mathcal{R}^R = &\mathbf{M}\frac{R^{n+1} - R^n}{\Delta t} \\ &- \theta\left[D_R \mathbf{K} R^{n+1} + \int N_i k_{on} R_i^{n+1}\, dx - k_{off}\mathbf{M} R^{n+1} + \int N_i k_s R_i^{n+1}\, dx \right] \\ &- (1-\theta)\left[D_R \mathbf{K} R^{n} + \int N_i k_{on} R_i^{n}\, dx - k_{off}\mathbf{M} R^{n} + \int N_i k_s R_i^{n}\, dx \right] \end{aligned} \tag{2.32}$$

$$\begin{aligned}\mathcal{R}^{R_i} &= \mathbf{M}\frac{R_i^{n+1}-R_i^n}{\Delta t}\\ &-\theta\left[D_{R_i}\mathbf{K}R_i^{n+1}-\int N_i k_{on}R_i^{n+1}\,dx+k_{off}\mathbf{M}R^{n+1}-\int N_i k_s R_i^{n+1}\,dx\right]\\ &-(1-\theta)\left[D_{R_i}\mathbf{K}R_i^{n}-\int N_i k_{on}R_i^{n}\,dx+k_{off}\mathbf{M}R^{n}-\int N_i k_s R_i^{n}\,dx\right]\end{aligned} \tag{2.33}$$

In particular, we solve it simultanoeusly at each time step with the Newton-Raphson algorithm. Our aim now is, given R^n and R_i^n, to find R^{n+1} and R_i^{n+1} such that $\mathcal{R}^R(R^{n+1},R_i^{n+1})=0$ and $\mathcal{R}^{R_i}(R^{n+1},R_i^{n+1})=0$. If we note $\Phi^k=\begin{pmatrix}R^{n+1}\\R_i^{n+1}\end{pmatrix}^k$, where k is the iteration counter index, and $\mathcal{R}=\begin{pmatrix}\mathcal{R}^R\\\mathcal{R}^{R_i}\end{pmatrix}$, the equation to solve is

$$\Phi^{k+1}=\Phi^k-\mathbb{K}^{-1}(\Phi^k)\mathcal{R}(\Phi^k) \tag{2.34}$$

starting by an initial approximation Φ^0 and having

$$\mathbb{K}=\begin{bmatrix}\dfrac{\partial\mathcal{R}^R}{\partial R^{n+1}} & \dfrac{\partial\mathcal{R}^R}{\partial R_i^{n+1}}\\ \dfrac{\partial\mathcal{R}^{R_i}}{\partial R^{n+1}} & \dfrac{\partial\mathcal{R}^{R_i}}{\partial R_i^{n+1}}\end{bmatrix}$$

where

$$\begin{aligned}\frac{\partial\mathcal{R}^R}{\partial R^{n+1}}&=\frac{\mathbf{M}}{\Delta t}-\theta D_R\mathbf{K}-\theta\int N_i\frac{\partial k_{on}}{\partial R}R_i^{n+1}\,dx+\theta k_{off}\mathbf{M}\\ \frac{\partial\mathcal{R}^R}{\partial R_i^{n+1}}&=-\theta\int N_i k_{on}\,dx-\theta\int N_i k_s\,dx\\ \frac{\partial\mathcal{R}^{R_i}}{\partial R^{n+1}}&=\theta\int N_i\frac{\partial k_{on}}{\partial R}R_i^{n+1}\,dx-\theta k_{off}\mathbf{M}\\ \frac{\partial\mathcal{R}^{R_i}}{\partial R_i^{n+1}}&=\frac{\mathbf{M}}{\Delta t}-\theta D_{R_i}\mathbf{K}+\theta\int N_i k_{on}\,dx+\theta\int N_i k_s\,dx\end{aligned}$$

At each time step n, our choice for the initial approach is $\Phi^0=\begin{pmatrix}R^{n+1}\\R_i^{n+1}\end{pmatrix}^0=\begin{pmatrix}R^n\\R_i^n\end{pmatrix}$ and we iterate over k the Newton-Raphson algorithm to find the next solution at $n+1$. Moreover, at every k we check whether $||\Phi^{k+1}-\Phi^k||<10^{-6}$ to ensure convergence. The scheme is presented as

Algorithm 1 Coupled system of R and R_i for any given time-step

1: Compute stimulus function $\longrightarrow k_S$
2: Set Φ^0
3: **while** convergence = false **do**
4: Get $\mathcal{R}^R$,$\mathcal{R}^{R_i}$ and $\mathbb{K}$
5: Compute $\Phi^{k+1}=\Phi^k-\mathbb{K}^{-1}\mathcal{R}$
6: **end while**

2.6 Coupling of the system of PDEs

Most of the equations in our model are coupled, this means, unknown variables appear in more that one equation. Recall that both momentum-balance equation and transport equations involved v and ρ_a or ρ_m. In fact, transport equation required $\tilde{v}$ but it was a function of v. We say that this system of PDEs is coupled. To solve it, at each time step we compute first the mechanic equation (with a given $\boldsymbol{\rho}_a^n$ and $\boldsymbol{\rho}_m^n$ from the previous time step) in order to find $\boldsymbol{v}^{n+1}$, and then we solve transport equations to find $\boldsymbol{\rho}_a^{n+1}$, $\boldsymbol{\rho}_m^{n+1}$. This method where, despite the equations are coupled, each equation is solved separately is called staggered method.

Algorithm 2 Main equations

1: **for** 1 to endTime **do**
2: Compute signaling equations $\longrightarrow R$ (eq 2.34)
3: Compute momentum-balance equation $\longrightarrow v$ (eq 2.22)
4: Compute change of reference frame $\longrightarrow \tilde{v}$ (eq 2.6)
5: Compute transport equations $\longrightarrow \rho_a$, ρ_m (eq 2.26)
6: **end for**

3 Results

3.1 Sensitivity analysis of active acto-myosin dynamics at fixed boundary

First, we can ask ourselves if we chose the correct parameters and how solutions are affected by them. Let us recall the mechanical equation for the actin network

$$\frac{\partial}{\partial x}\left(\mu\frac{\partial v}{\partial x}+\xi\rho\right)=\eta v \tag{3.1}$$

The parameters involved here are viscosity μ, contractility ξ and friction η. All these parameters have been studied in the lab and are known for different type of cells. However, by modifying them we can detect some other interesting combinations and also verfy our model. Here we performed a sensitivity analysis by changing parameters around the default values, which initially were $\mu = 10$, $\xi = 0.1$, $\eta = 1$ (see Table 1 for final values used). Beside this, we can state convenient boundary conditions in order to focus on what we need. In this case, we keet the cell attached to the substrate, so $v_{cell} = 0$. We also imposed Dirichlet boundary condition for the velocity of actin flow, namely $v = 0$ at the rear edge and $v = -0.1$ at the front (note its negative sign due to the right-to-left direction of the flow). These conditions allow a better and easier analysis of what we want to see.

We study initially how the velocity of the actin network is affected when varying the parameters. Figure 3.1 shows this velocity along the cell at the end time ($t = 3000$s). Since there are too many combinations for all three quantities, here we pick just a few interesting combinations, which contain default values. For three different values of viscosity $\mu = 3$, $\mu = 10$ and $\mu = 30$ and two different elasticity constants $\xi = 0.1$ and $\xi = 0.01$, we show v depending on the friction taking the values $\eta = 0.05$, $\eta = 1$ and $\eta = 5$.

Results show that in general, the velocity of the actin network tends to zero earlier when friction is higher. For the lowest values of friction, velocity decrease constantly. Moreover, if we increase contractility with low friction, actin velocity do not decrease along the cell, but even increases. Finally, it can be deduced that increasing viscosity reduce the velocity variation and it decreases straighter. In fact, since our boundary conditions impose velocity in both edges, with higher

viscosity the velocity graph tends to a straight line.

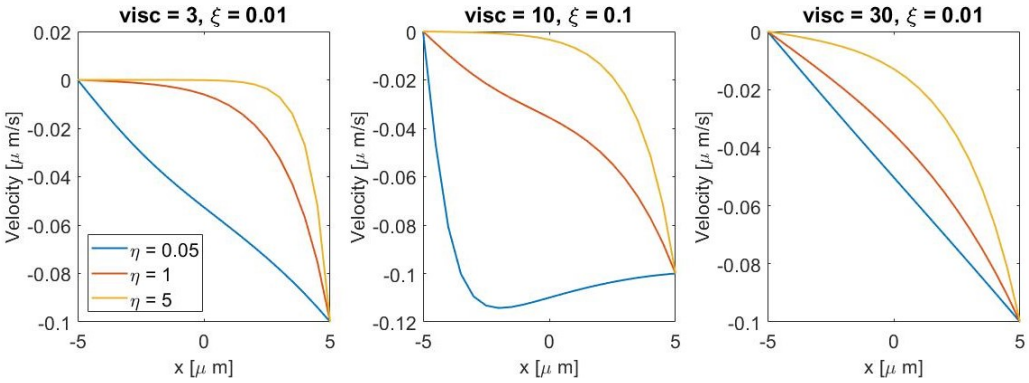

Figure 3.1: Velocity profiles of the actin meshwork for three different pair of values of viscosity μ and contractility ξ. For each μ and ξ we plot v on three substrates with different friction η.

At the beginning of the chapter we considered just the mechanical equation for the actin network. However, velocity v is involved in actin and myosin transport equations. That is why we also analyse how actin and myosin densities are affected when changing some parameters. Figure 3.2 shows the plots for the actin and myosin densities, as well as the actin network stress, for different friction parameters. We show them only for one pair of viscosity and contractility because other values are quite similar.

Results show that the lower friction is, v is higher, and therefore there is more convection so both densities augment in the back. Despite that, while myosin do always accumulate at the rear edge, for high values of friction, actin density still grow at the front. Regarding to tension, the higher the friction is, we note higher stress. The negative sign is due to the direction it is applied, a positive stress means a traction force and a negative stress means there is a compression force.

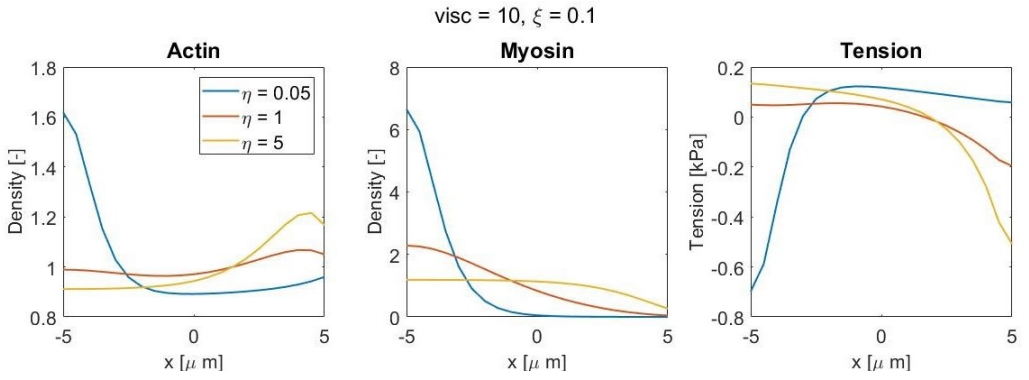

Figure 3.2: Actin and myosin concentration and stress for a given viscosity $\mu = 10$ and contractility $\xi = 0.1$. Each variable is shown for different values of friction η.

3.2 Early cell spreading

Once a sensitivity analysis is done, we can proceed to test numerically how the cell migrates following our model. Here we prove the model on the early events in the cell spreading, this is, we place a cell on the extracellular matrix with no polarization. A no-polarized state is given by considering constant friction and no external stimulus, taking the free polymerization velocity $v_0^p = 0.55\mu$m/s equal in both edges.

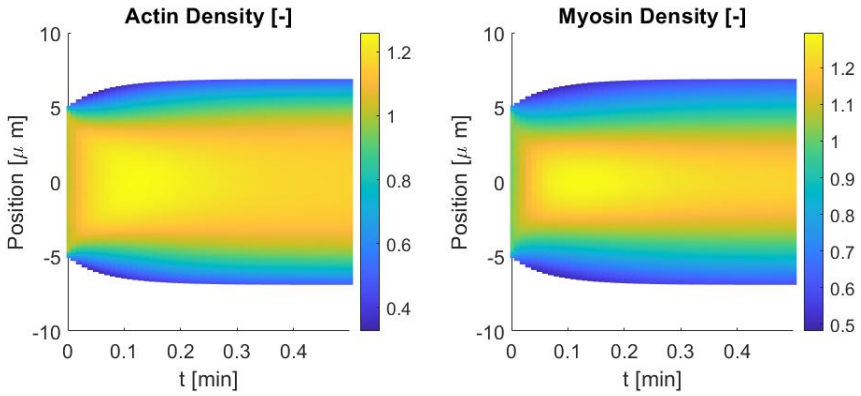

Figure 3.3: Concentration of actin and myosin in the cell for 30 seconds.

Figure 3.3 shows the symmetry on actin and myosin concentration, which is given by the fact that there is no stimulus to motivate the cell to move. We also note the cell spreads symmetrically until the membrane tension compensates the polymerization force. This behaviour was expected and it has been shown also in the lab [13]. In fact, here we do not take into account the numerous folds the cell membrane actually has. If we considered them, the cell would extend freely (with no membrane tension) until it was totally unfolded. In our experiment the cell length become stable at 13.81μm long. We show the variables at the steady state in figure 3.4, where we run the simulation for 100 seconds. We show actin and myosin concentarions in the cell, as well as their evolution at the edges along time. We also plotted in figure 3.4 the actin velocity, which is also symmetric and centripetal, this is, actin flows from the edges to the center. Symmetry is also given by the boundary conditions on the mechanical equations since we imposed the same membrane tension σ_m in both edges. Finally, we show in figure 3.4 the evolution of the actin protrusion velocity at both edges. We note the velocity decreases and stabilize. This is due to the cell membrane that exerts an opposite force to actin filament growth. At the steady state, the protrusion velocity, which pushes the cell membrane outwards, is compensated with the actin inward flow.

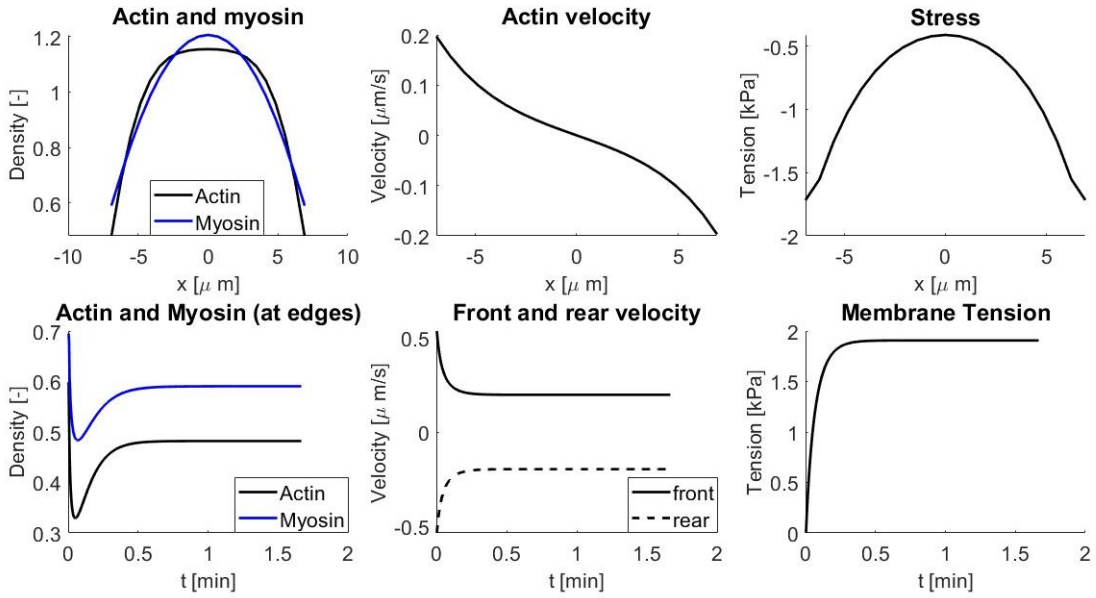

Figure 3.4: Actin and myosin densities inside the spreading cell. Actin velocity inside the cell. Stress of the actin meshwork along the cell. Actin and myosin concentration at edges for 100 seconds. Protrusion velocity of F-actin at leading and rear edge along time. Membrane tension σ_m during time.

3.3 Polarization of signaling cues

One way to initialize polarization is by external signaling. Here we show the results of solving the coupled system of GTPases proteins (equation 2.5.3), which guide the cell when is starts moving. We plot both active GTPases concentration R [molecules/length] and inactive ones R_i, as well as the external stimulus k_S. We consider first constant initial conditions equal to one for both active and inactive GTPases and a graded stimulus defined in equation 2.15 for 20 seconds. We show this on figure 3.5 and as expected, active GTPases proteins polarize according to the external stimulus. A remarkable property is that this polarized state is maintained indefinitely, even when we remove the stimulus. We see this by plotting the molecules concentration until $t = 200$s.

We next ask whether our cell model is sensitive to new incoming signals. Here we study this by adding a new identical stimulus toward the other direction. The response of GTPases is that they do polarize on the other extreme, according to the new stimulus. Here we add k_S at $t = 200$s until $t = 225$s but on the other side. Results show that, in fact, active GTPases change their orientation to the other edge. We show this on figure 3.6.

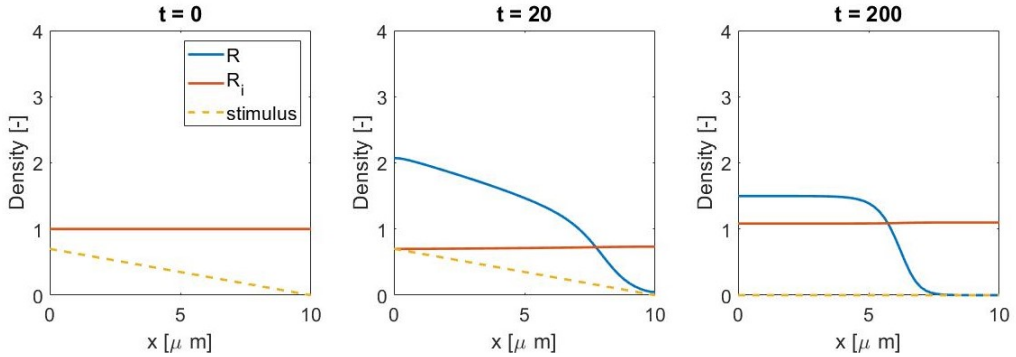

Figure 3.5: Evolution of active and inactive GTPases concentration according to an external stimulus k_S. Despite k_S is applied for only 20 seconds, R stays in a polarized state.

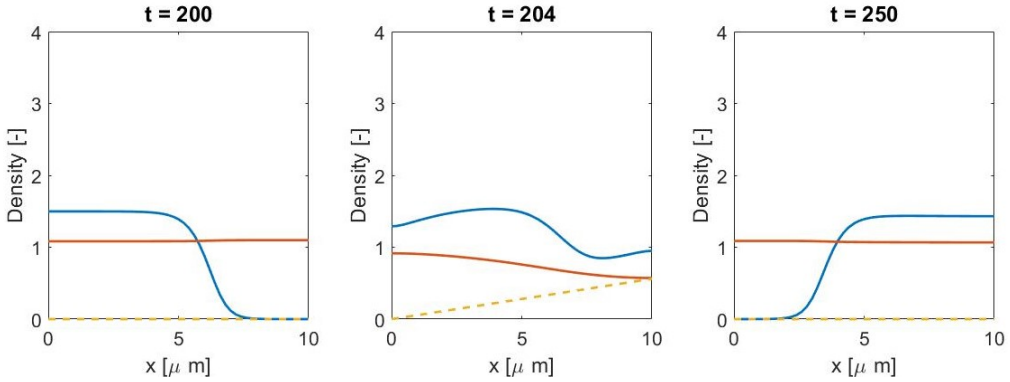

Figure 3.6: Evolution of GTPases concentration when applying an opposite stimulus to a polarized configuration.

Finally, we simulate the GTPases polarization with no external stimulus k_S, but with a random initial condition for the active GTPases. We observe that they can polarize either rightwards or leftwards. We also note that sometimes, if the initial condition presents equal peaks in both sides, active GTPases will not be able to decide which side to polarize so concentration will stabilize being constant. We see all this cases on figure 3.7.

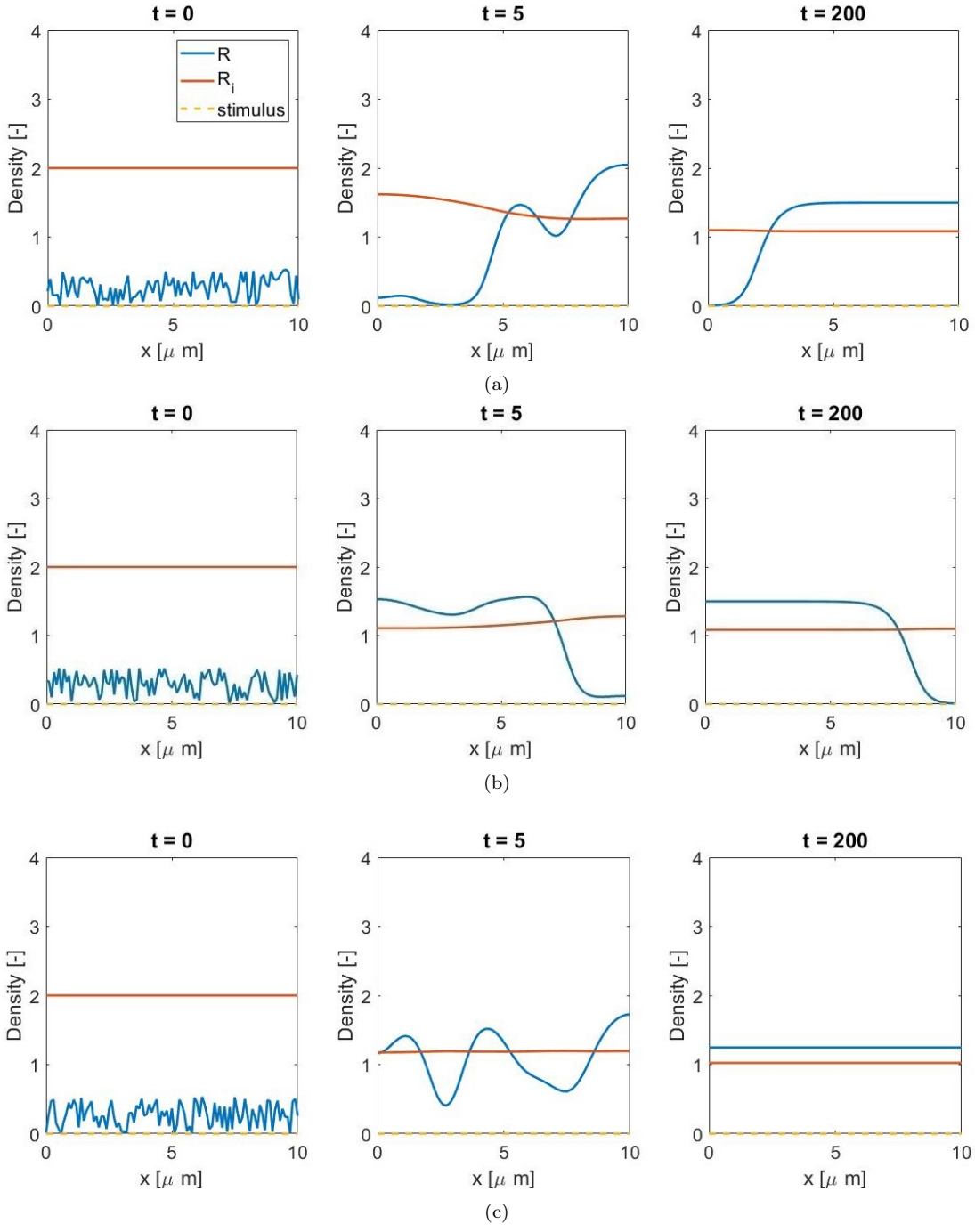

Figure 3.7: (a)Rightward polarization of active GTPases from a random initial condition. (b) Leftward polarization of active GTPases from a (different) random initial condition. (c) No-polarized steady state of active GTPases.

A similar way to obtain a random polarization is by considering constant initial conditions for R and R_i and a random k_S for the first seconds as shown in figure 3.8. The initial conditions we considered were $R(x,0) = 0.8$ and $R_i(x,0) = 1$.

With this initial conditions, we ran 100 times the code. 31 times R polarized to the right, 36 times to the left and 33 times they stayed stable and did not polarize. When we considered both R and R_i equal to one at $t = 0$, more than 40% of the times R remained stable and did not polarize, that is why we decided to work with lower initial values of active GTPases.

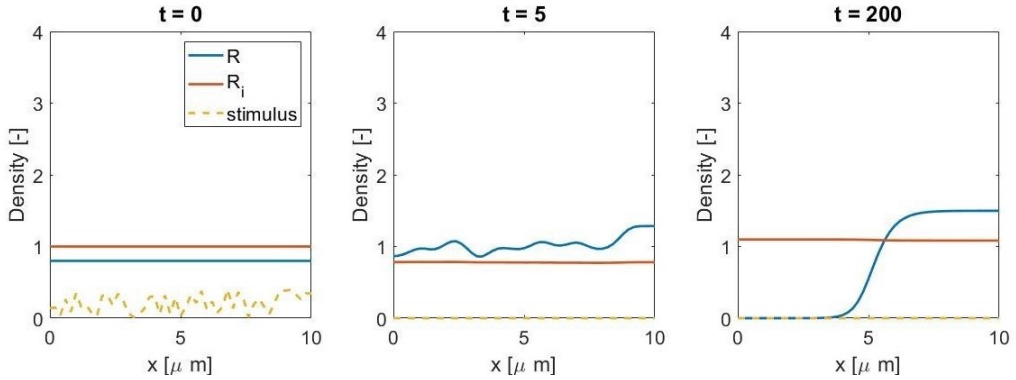

Figure 3.8: Polarization of active GTPases due to a random external stimulus applied at first seconds.

3.4 Initial polarization and migration enhanced by signaling

So far we have modeled the principal mechanisms that develop cell migration: retrograde flux of actin as well as protrusion generated by F-actin. Moreover, we considered protursion velocity as a function of active GTPases in equation 2.17, which increase F-actin growth and induce polarization. In this section we stimulate the plasma membrane with an external signal in order to generate a gradient of active GTPases. With a different concentration of R on edges, there will be a higher protrusion velocity on one side and the cell will start to move.

A crucial advantage of implementing polarization by GTPases cycles between active and inactive forms is that we can lead the cell through external signals. Let us consider now the whole motile cell model. First of all, we show that we can guide the cell from the beginning by activating the external stimulus for a few seconds. We show this on figure 3.9 by plotting actin and myosin densities during some time with opposite stimulus. Given that both situations are symmetric, we can choose either one or the other to study. Here we take the rightward moving simulation and we run it for 100 second to ensure a steady state. On figure 3.10 we show the behaviour of the principal components of the cell.

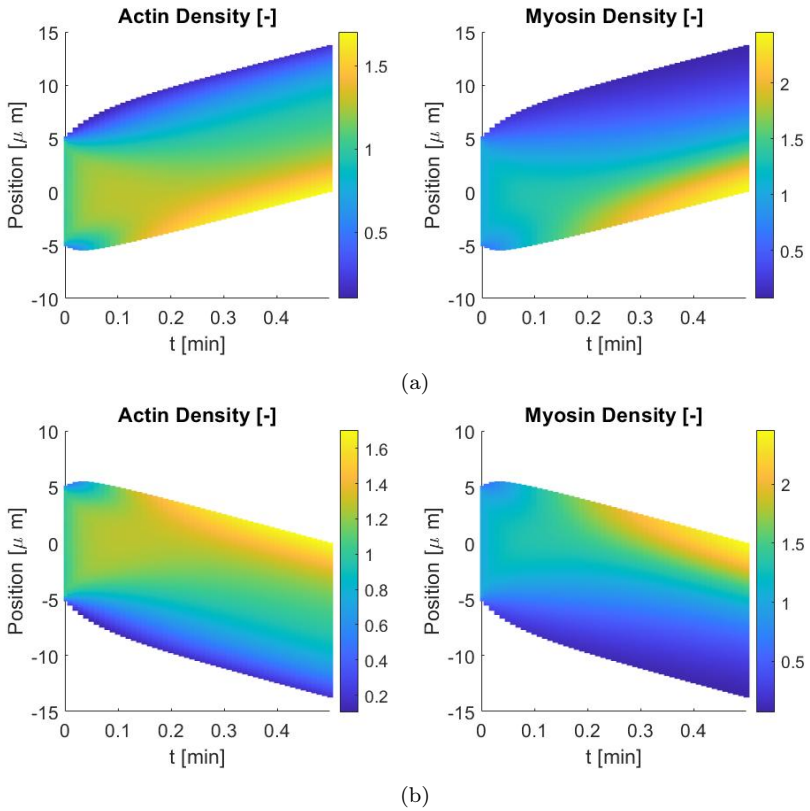

Figure 3.9: (a) Actin and myosin densities of the cell initially stimulated with a right-oriented external signal. (b) Same but with a left-oriented external stimulus.

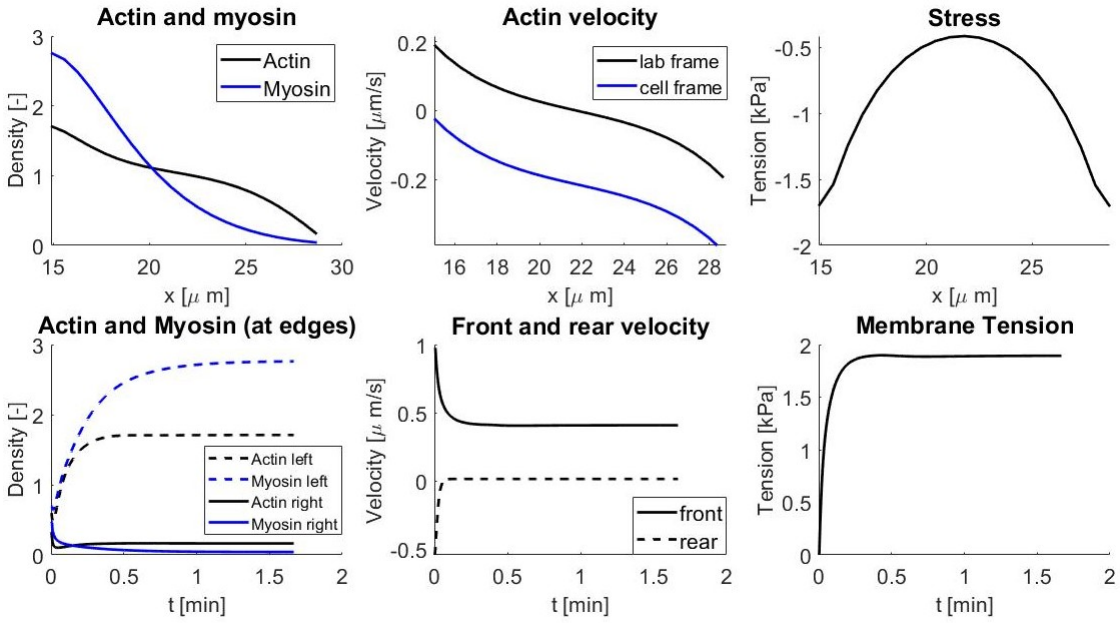

Figure 3.10: Actin and myosin densities inside the rightward polarized cell. Actin velocity inside the cell. Stress of the actin meshwork along the cell. Actin and myosin concentration at edges for 100 seconds. Protrusion velocity of F-actin at leading and rear edge along time. Membrane tension σ_m during time.

We can see in figure 3.10 how actin and myosin perform in our model, starting from the same initial condition (a cell-length random vector) and how evolve. They rapidly decrease at the front part of the cell, while both, actin and myosin, increase in the rear due to the retrograde flow. When they stabilize, actin gets a concentration of 1.71 in the rear and 0.16 at the front, while myosin reaches 2.76 on the rear and 0.04 at the front. If there are no external interference, this distribution will remain stable onward.

The velocity of the actin network flux inside the cell when it becomes stable is shown in the figure 3.10 in the lab and cell frame. Actually, the difference between both velocities is the velocity of the cell. In the cell frame, the velocity on the rear is -0.01μm/s, while at the front it is -0.41μm/s. We also show other variables like the stress, which increases on the edges (on absolute value), or the protrusion velocity on both edges. Here, the leading edge reaches 0.41μm/s while the rear one is 0.015μm/s because of the depolymetization rate. We also note that membrane tension increases until the cell length stabilizes. We show this on figure 3.11. The very first thing we note is, despite the cell initially is 10μm long, it elongates until 13.79μm. This is where the free velocity of polymerization is compensated with the resistance of the cell membrane (at 1.89kPa), which is proportional to the cell length growth. We also computed the velocity of the cell, which increases rapidly in the initial seconds until it stabilizes at 0.21μm/s, where the cell travels at constant velocity.

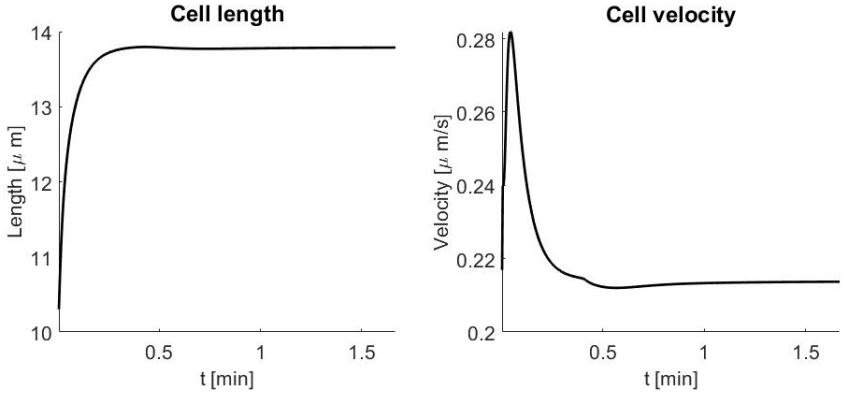

Figure 3.11: Length and velocity of the right-moving cell for 100 seconds.

In section 3.2 we observed GTPases do polarize with no external stimulus if a random initial condition was settled for active forms R. We asked ourselves if the cell also polarize and choose a side to move. Results show that, for a random initial configuration of R, the cell also polarize towards the side where GTPases density is higher. We see this in figure 3.12. Here we only plotted the first 30 seconds in order to analyse better the initial process. We can see that, since a random initial condition requires a low value of R [6], it needs some seconds to achieve a high enough value and start to move. Actually, the time it takes R to be big enough depends on how the initial R develop. In 3.12, it takes around 7

seconds to start moving, where the cell shrink due to retrograde flow. At that time, active GTPases concentration was 0.65 and it stabilized at 1.71, in units of molecules/length. At the end time, the cell was 13.88μm long and it traveled at 0.2μm/s speed to the right.

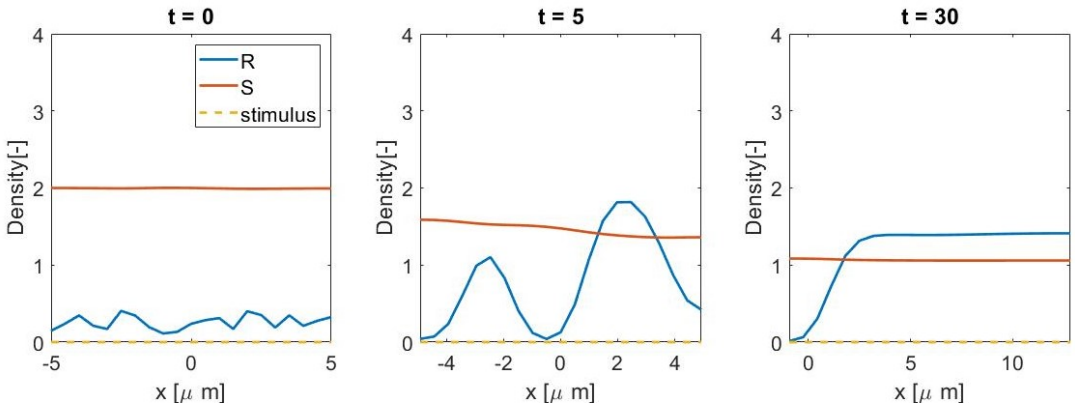

(a)

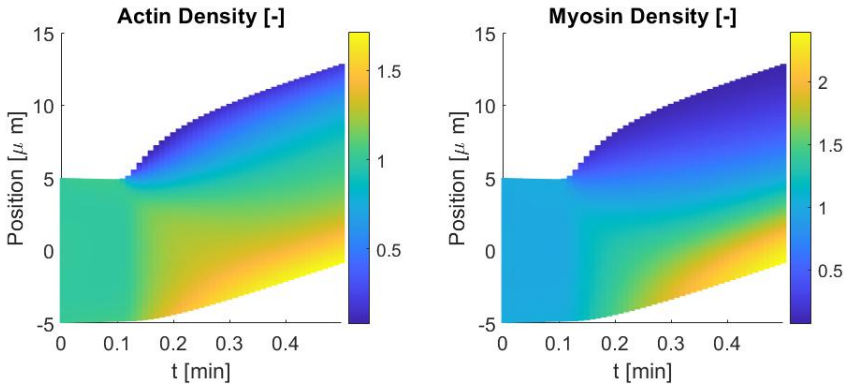

(b)

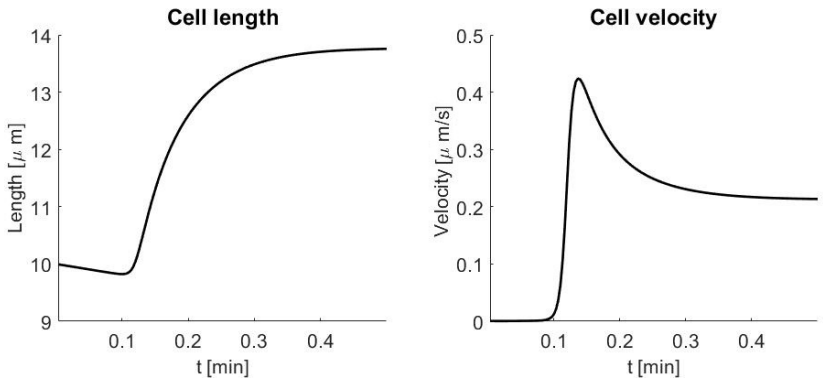

(c)

Figure 3.12: (a)Evolution of active and inactive forms of GTPases proteins at three different moments starting from a random configuration of active ones. (b)Actin and myosin concentration along space ans time. (c) Cell length ans cell velocity

Finally, we were interested in how the cell behaves under two different external signals. First, we applied the stimulus k_S defined in the equation 2.15 to the left and, after 100 seconds, we applied the same stimulus rightwards for 20 seconds.

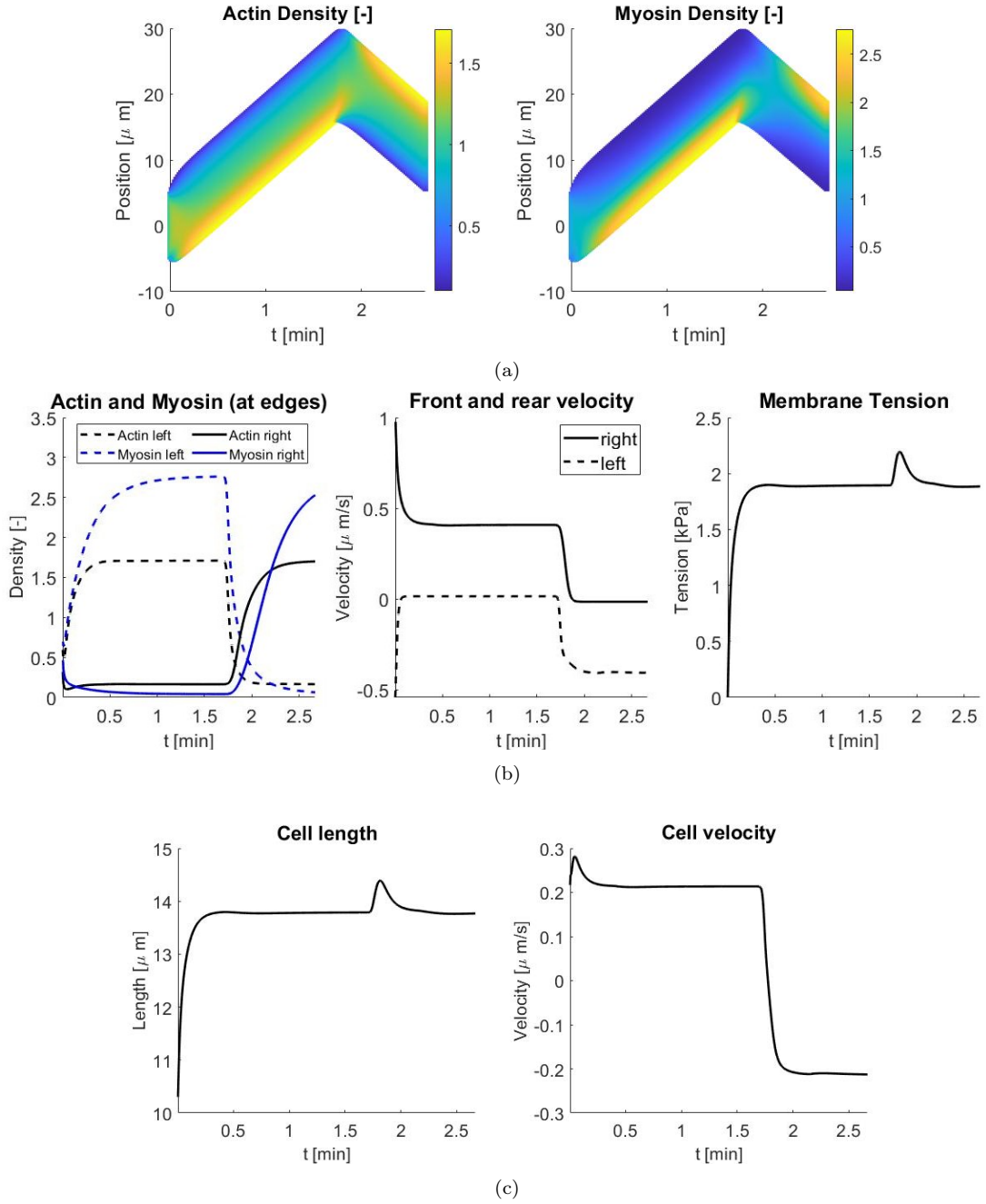

Figure 3.13: Moving cell after apply two external stimulus at $t = 0s$ and $t = 100$s. (a)Actin and myosin concentration along space and time. (b) Actin and myosin density at the right and left edge of the cell during time. Protrusion velocities at both edges: when the cell moves rightwards the right edge is the front one and when the cell moves leftwards the left edge is the front one. Membrane tension during time. (c)Cell length and cell velocity of the moving cell.

Results show that it takes to the GTPases ~ 2 seconds to reach a high enough

concentration to change the cell direction. However, the cell reacts instantaneously and it only needs around 16.8 seconds to arrive to the cruising speed 0.2μm/s on the other direction. We also note an increase of the cell length when modifying its way. The cell length gets 14.7μm, which is a 6.3% more than its travel length. The increase on the cell length involve an increase on the membrane tension since they are proportional. On figure 3.13 we also show how actin and myosin arise and fall on both edges when we add an opposite-directed external stimulus. We note as well the switch between front and rear protrusion velocity. The front side always stabilize at 0.41μm/s.

3.5 Initial polarization and migration enhanced by friction gradients

The other method we study here to initialize the cell motion is durotaxis, this is, the ability of cell to follow gradients of substrate friction. Until now we have been using $\eta_0 = 3$ kPa $\cdot$ s/μm as a friction parameter. Let us consider now an extracellular matrix with a non-constant stiffness $\eta(x)$. The function $\eta(x)$ we use here is a linear gradient, whose slope or direction can be modified to obtain different outcomes. Results reproduce what has been seen in the lab [2]: with no external signaling, the cell follows the gradient towards the stiffer region. Since we are considering just movement because of friction gradients, we are using a constant free polymerization velocity $v_0^p = 0.55$ at both edges.

We start our experiments with a short sloped gradient, taking $\eta(x) = \eta_0 + 0.05x$. Figure 3.14 shows actin and myosin density in the cell while the cell moves. We also show the stiffness of the substrate, where the thicker the more friction there is. Despite the cell spreads normally until its length is 13.83μm, we note that the small stiffness variation do not allows the cell to move at high speed. In fact, $v_{cell} = 0.009\mu$m/s. Other variables of the model are comparable to the stationary cell ones, showed in figure 3.4.

Although we are considering a small gradient on the substrate friction, we could ask whether the cell behaves different depending on the position we put it. Hence, we also place the cell on $x = 100$. Results show that the cell spreads up to a bigger steady length but its velocity is considerably smaller. Actually, these results were expected because we already know that higher friction lead to slower retrograde flux. On figure 3.15 we show the cell spreading until it is 14.78μm and moving at 0.003μm/s.

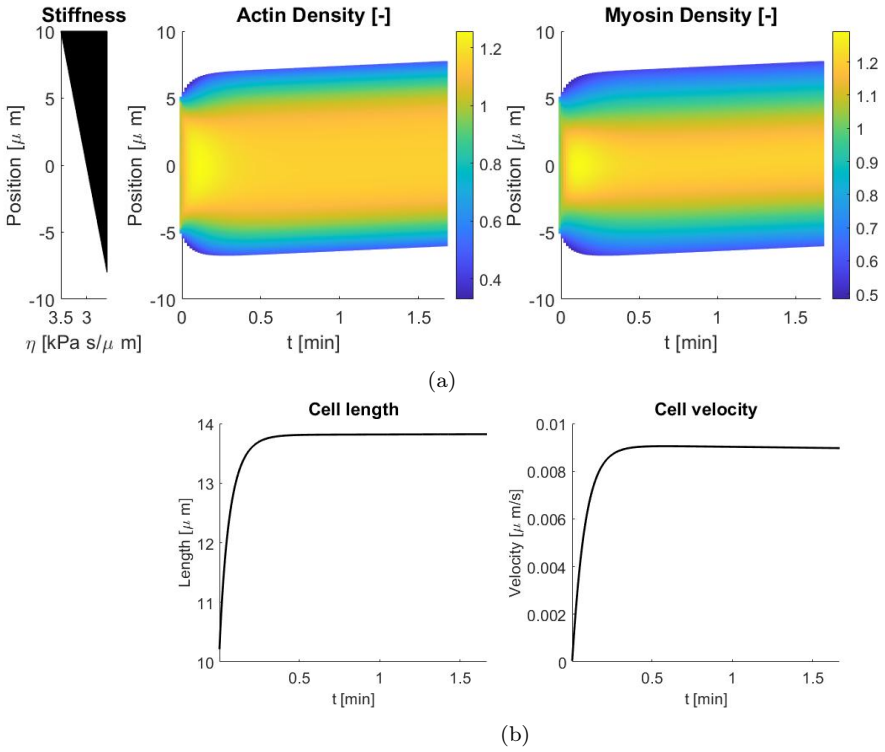

Figure 3.14: (a)Actin and myosin concentration of a cell placed on $x = 0$ and a substrate with variable friction $\eta(x) = \eta_0 + 0.05x$. (b) Cell length and velocity of the cell for 100 seconds.

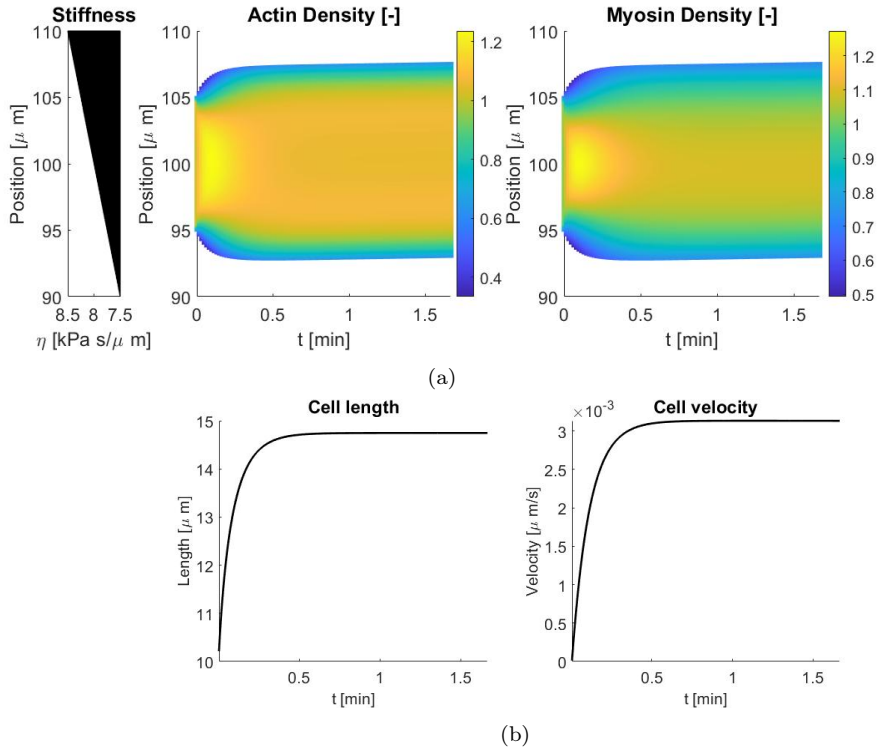

Figure 3.15: (a)Actin and myosin concentration of a cell placed on $x = 100$ and a substrate with variable friction $\eta(x) = \eta_0 + 0.05x$. (b) Cell length and velocity of the cell for 100 seconds.

We also executed simulations on a matrix with a bigger stiffness gradient. In particular, we show in figure 3.16 the performance of the cell on a substrate with friction $\eta(x) = \eta_0 + 0.5x$. The cell also follows the increasing resistance, but we note a non-symmetric actin and myosin profiles, as well as a velocity increase up to $v_{cell} = 0.03\mu$m/s and its length, which reaches 14.6μm at the end of the simulation.

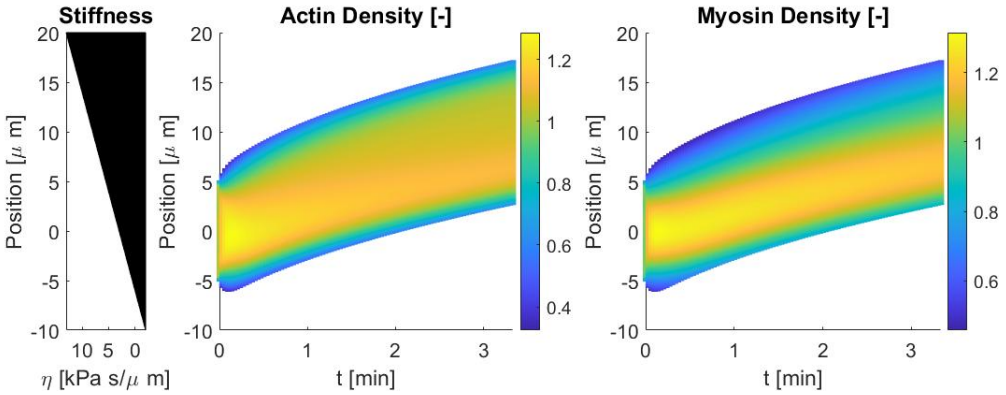

Figure 3.16: Actin and myosin concentration of a cell on a substrate with variable friction $\eta(x) = \eta_0 + 0.5x$.

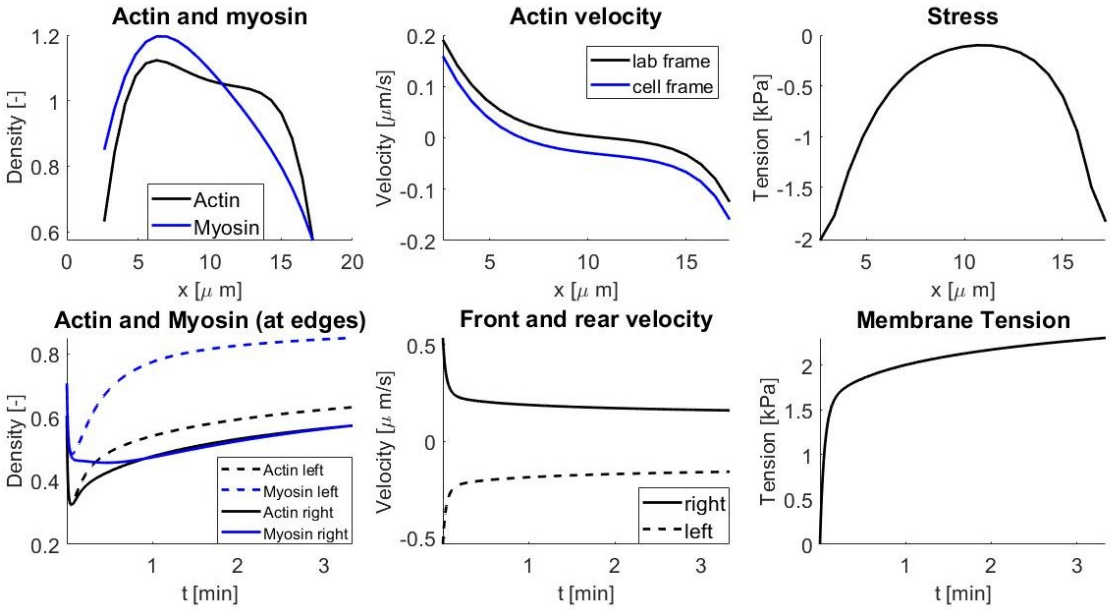

Figure 3.17: Actin and myosin concentration inside the cell. Actin velocity on the lab frame and cell frame. Stress of the actin meshwork. Evolution of actin and myosin concentration on edges for 200 seconds. Front and rear protrusion velocity. Membrane tension evolution.

On figure 3.17 we show the actin and myosin concentration profiles and their evolution on cell edges. We also plot the stress of the actin network and protrusion

velocities on edges. Although protrusion velocities are equal on both sides because we are using the same v_0, we note they slightly decrease. This is a consequence of the increase of the membrane tension, which is also a result of the increase of the cell length.

We ran the simulation of the cell on a high stiffness gradient for 200 seconds (figures 3.16 and 3.17). However, the cell do not arrive to a steady state because at the end time the cell still spread and its velocity was not constant. In our simulation with a high friction matrix, the cell takes more than 800 seconds to reach a steady state. We can get this result also by placing the cell in positions with higher stiffness, instead of setting the cell on the origin. Here, we set the cell at $x = 35$, where it migrates with constant length and velocity. The cell length is 14.54μm and it travels at 0.01μm/s. We show this on figure 3.18. Model variables are comparable to the steady state results, shown on figure 3.4.

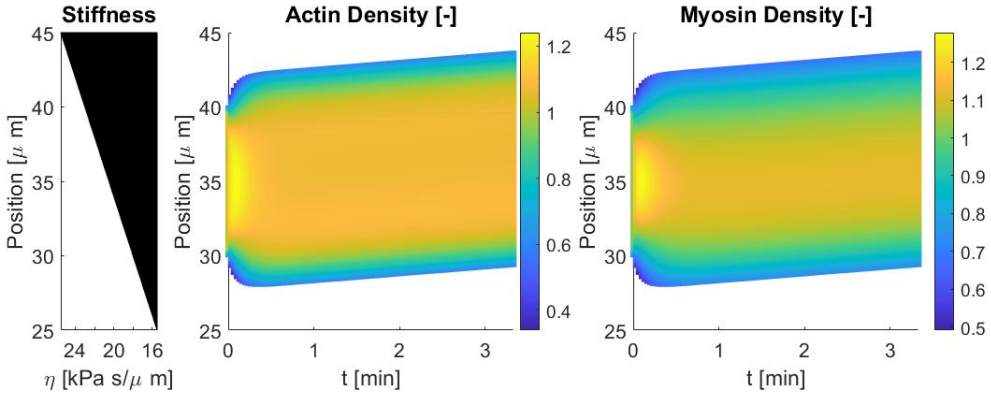

Figure 3.18: Actin and myosin concentration of a cell on a substrate with variable friction $\eta(x) = \eta_0 + 0.5x$ placing the cell on $x = 35$.

We do not show here the case where the gradient increases to the left, but the cell also follows the stiffness gradient going leftwards.

3.6 Tug of war between adhesion forces and signaling-based migration

In this final section we activate both ways to initiate the cell migration: the external signaling and the gradient substrate friction. We do not only activate them simultaneously, but we will also consider first a friction gradient and then we will add an external stimulus.

When we have a non-constant friction substrate and we turn on the signaling towards the decreasing gradient, we note the cell does not follow the stiffness anymore, but obeys our external stimulus. This occurs due to a higher protrusion

velocity over the retrograde flux. Despite the intern actin flux pushes the cell because of the friction gradient as seen in section 3.5, GTPases concentration induce actin polymerization, and so protrusion velocity. Since we develop $v_0^p(R)$ by ourselves, we do not refuse that with distinct values of polymerization velocity, or a higher stiffness slope, the cell would move differently. Here we impose the friction function $\eta(x) = \eta_0 + 0.5x$ on the extracellular matrix. Figure 3.19 shows the cell moving because of the leftward external signaling.

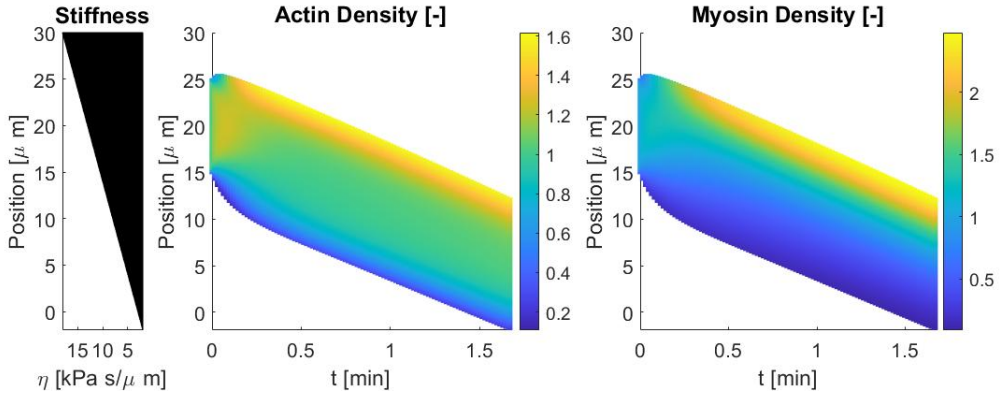

Figure 3.19: Moving cell under on a non constant matrix and subjected to an leftward external stimulus.

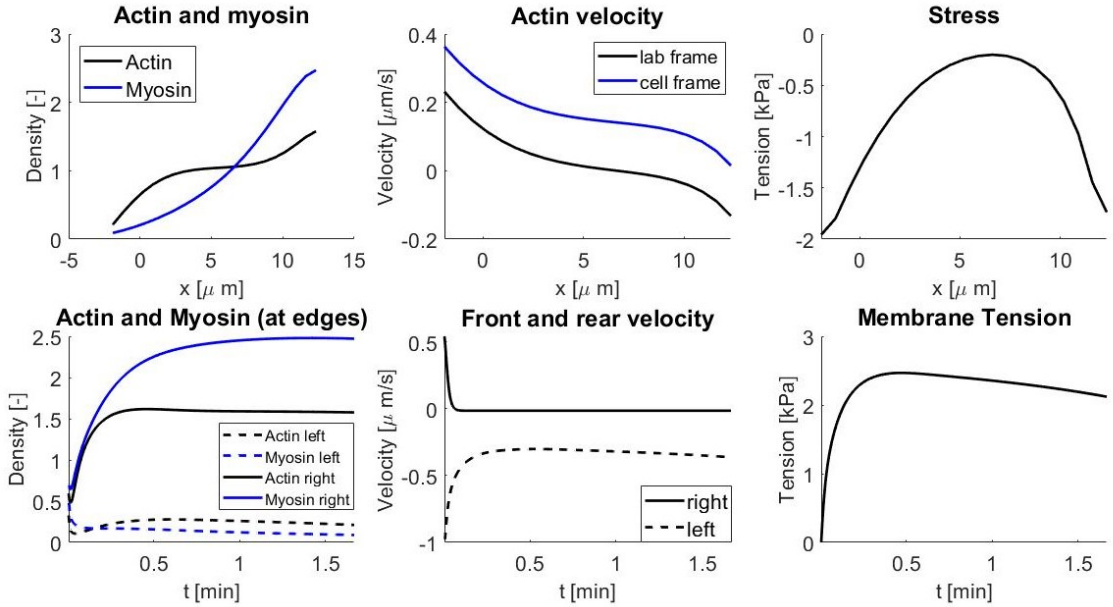

Figure 3.20: Actin and myosin densities inside the cell. Actin velocity inside the cell. Stress of the actin meshwork along the cell. Actin and myosin concentration at edges for 100 seconds. Protrusion velocity of F-actin at leading and rear edge along time. Membrane tension σ_m during time.

Note that, since the cell now does not move to more rigid zones, we place the cell on $x = 20$ so the it does not enter a negative-friction region, which makes no physical sense. The cell initially spreads until it is 14.9μm and then, its length decrease because it is moving to regions with less friction. However, the cell velocity remain constant at -0.14μm/s, which is less than the velocity obtained with constant friction in section 3.4. This makes sense because now we have a contrary force due to friction. On figure 3.20 we show actin and myosin densities profile, which are not symmetric anymore, but increase in the back of the cell. We plotted also actin velocity and its stress.

Finally, if we activate the external signaling when some time has passed, we note how the cell turns around according to the stimulus direction. In particular, here we show how the cell perform on a matrix with friction $\eta(x) = \eta_0 + 0.5x$ for 100 seconds, and then we apply the signaling leftwards for 50 more seconds. Figure 3.21 shows the cell turnover, while figure 3.22 shows the difference on actin and myosin concentration at edges and the membrane tension when applying the external signal. We also plot protrusion velocity, which is equal on both sides until we activate the stimulus.

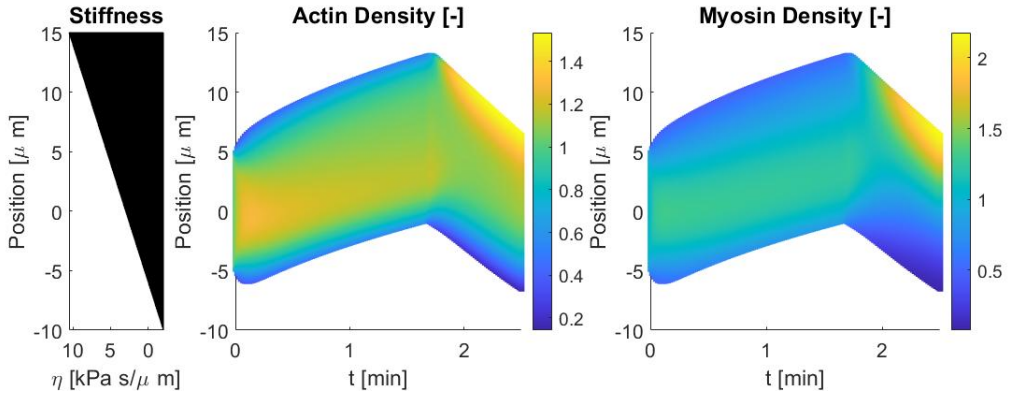

Figure 3.21: Evolution of actin and myosin concentration on a substrate with non-constant friction for 100 seconds. Then, an external signal is applied leftward for 50 seconds.

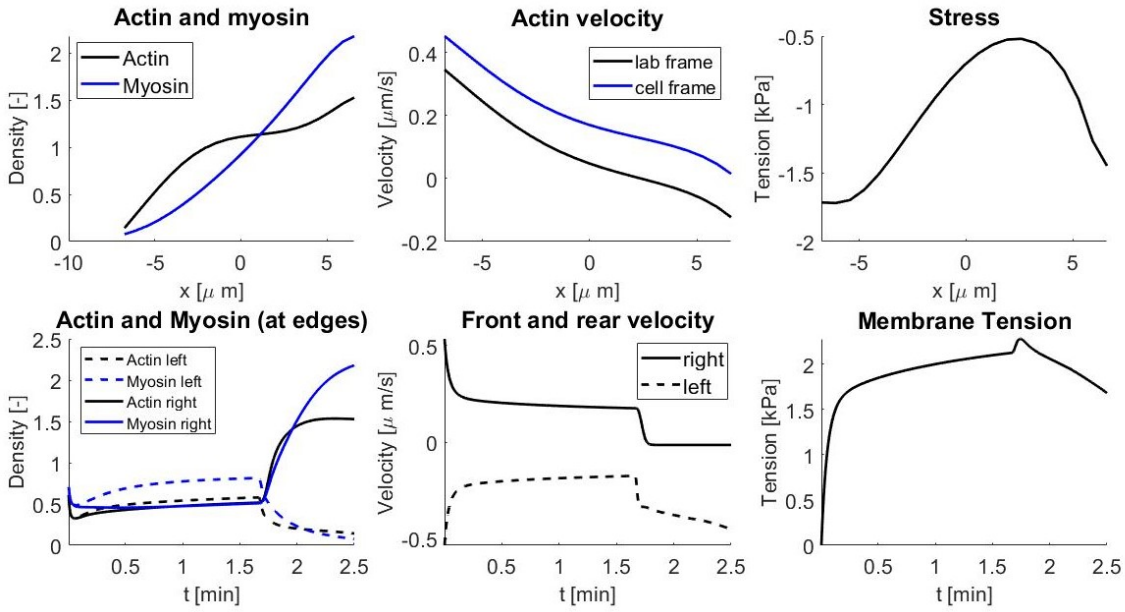

Figure 3.22: Actin and myosin concentration profile at the end time. Actin velocity. Stress of the actin network. Evolution of actin and myosin concentration at the edges: we observe that the leftward stimulus pushes both proteins to the back part of the cell. Right and left protrusion velocity. Membrane tension.

4 Discussion and future work

The aim of this bachelor's degree thesis was to study the principal components of cell migration and develop a model that simulates these processes. We also had implement sensitive polymerization to GTPases and proved that our model respond accurately to external stimulus, which let us polarize and guide the cell. Finally, we proved our model in different situations in order to see if it performed as expected.

We developed a model that let us recreate the motion of a cell by the main mechanisms of cell motility: edges protrusion, retrograde flow and myosin contractile stress. Governing equations of actin and myosin evolution are essentially partial differential equations following force balance principle and conservation of mass. This all, together with the constitutive relations we thought best fit reality, allowed us to elaborate the model we latter used to simulate cell migration. In addition, evolution of GTPases proteins, that has been described as a coupled bistable system of PDEs with nonlinear source terms, were implemented in our model.

Solving the equations has been also a relevant part of the work. Since resolution had to be computational, it was important to choose the numerical methods that better solutions give, based on stability and good convergence. Here we used a finite element scheme to approximate all the partial differential equations because its easy implementation and quickly adaptation for different purposes. Furthermore, boundary conditions can easily settled when using finite element methods. Numerical solutions we get were accurate and reliable, so we need no stabilization methods or mesh refination. For the time integration of the equations, we used Crank-Nicolson method because it is implicit, which means it is unconditionally stable, and second order.

Here, we initially did a parametric analysis and study the effect of viscosity, friction and contractility on the actin network velocity. We observed that lower friction or higher contractility allows a higher velocity of F-actin inside the cell. Otherwise, higher viscosity of the gel hinders variations on the velocity. We first proved our model with no polarization. The cell was placed on the extracellular matrix and it spread as it did in [13]. We also observed that the cell length increased when it was totally spread if the cell was placed on a higher stiffness substrate. Regarding to polarization, we accomplish implementing the cell stimulation via GTPases kinetics and their influence on actin polymerization. The

cell was observed to maintain its polarized state when the the external signal is removed. Actually, this is a property of the GTPases bistable system, which preserve active concentration on one edge as a stable state. However, we have seen that although the cell is already moving, it is sensible to new external signaling and it can change its direction towards a new way. We finally proved that the cell can also initiate motion by a randomly generated signaling, which initiates also a random directed movement of the cell. We have seen that our cell model is able to move because friction gradients on the cellular matrix as seen in [2]. On small friction gradients, the cell moves at constant length and low velocity. On the other hand, when we considered bigger gradients, the cell starts moving fast and then it moves slower while it spreads. It arrives at a steady state, which can be also achieved if we place the cell on higher stiffness positions. Finally, this work compare both stimulus, the external signaling to polarize GTPases and a friction gradient on the substrate, by activating them at once. Results show that in our model, polarization via membrane GTPases signaling prevails over friction gradients. This can be explained because the way we define free polymerization velocity, which is function of active GTPases.

We consider that further interactions, such as considering the actin network as elastic or testing different parameter values, would be interesting when modelling cell migration. Different definitions of polymerization velocity as a function of active GTPases would also contribute to create more reliable and solid models. Beside this, a great advance would be to take the step to a two-dimensional model, so we could study accurately the shape of the cell. In this dissertation we just showed a small part of what computational modelling applied to biology comprises, and in particular, to cell migration. We believe that this is an important field because the progress it can contribute to. We know cell migration is essential in vital processes like cancer, embryonic development and wound healing. Thus, we encourage in pursuing mathematical developments on this line of work.

Bibliography

[1] Gracheva-OthmerMaria E. Gracheva and Hand G. Othmer. 2004. A Continuum Model of Motility in Ameboid Cells. *Bulletin of Mathematical Biology* 66, pp. 167-193.

[2] Raimon Sunyer, Vito Conte, Jorge Escribano, Alberto Elosegui-Artola, Anna Labernadie, Léo Valon, Daniel Navajas, José Manuel García-Aznar, José J. Muñoz, Pere Roca-Cusachs, Xavier Trepat. 2017. Collective cell durotaxis emerges from long-range intercellular force transmission. *Science* Vol. 353 (6304), pp 1157-1161.

[3] Kamila Larripa, Alex Mogilner. 2006. Transport of a 1D viscoelastic actin–myosin strip of gel as a model of a crawling cell. *Physica A* no. 372, pp 113-123.

[4] Boris Rubinstein, Maxime F. Fournier, Ken Jacobson, Alexander B. Verkhovsky and Alex Mogilner. 2009. Actin-Myosin Viscoelastic Flow in the Keratocyte Lamellipod. *Biophysical Journal* Vol. 97, pp 1853–1863.

[5] Alexander B. Verkhovsky, Tatyana M. Svitkina and Gary G. Borisy. 1998. Self-polarization and directional motility of cytoplasm. *Current Biology*, 9:11-20.

[6] Yoichiro Mori, Alexandra Jilkine, and Leah Edelstein-Keshet. 2008. Wave-Pinning and Cell Polarity from a Bistable Reaction-Diffusion System. *Biophysical Journal* Vol. 94, 3684–3697.

[7] Alex Mogilner and Leah Edelstein-Keshet. 2002. Regulation of Actin Dynamics in Rapidly Moving Cells: A Quantitative Analysis. *Biophysical Journal* Vol. 83, 1237–1258.

[8] Gaudenz Danuser, Jun Allard and Alex Mogilner. 2013. Mathematical Modeling of Eukaryotic Cell Migration: Insights Beyond Experiments. *Annual Review of Cell and Developmental Biology* 29:501-28.

[9] Nils C. Gauthiera, Marc Antoine Fardina, Pere Roca-Cusachsa, and Michael P. Sheetza. 2011. Temporary increase in plasma membrane tension coordinates the activation of exocytosis and contraction during cell spreading. *Proceedings of the National Academy of Sciences* Vol. 108, no. 35.

[10] T. Putelat, P. Recho, and L. Truskinovsky. 2018. Mechanical stress as a regulator of cell motility. *Phyisical review* E 97, 012410.

[11] Bruno Pontes, Pascale Monzo, Laurent Gole, Anabel-Lise Le Roux, Anita Joanna Kosmalska, Zhi Yang Tam, Weiwei Luo, Sophie Kan, Virgile Viasnoff, Pere Roca-Cusachs, Lisa Tucker-Kellogg, and Nils C. Gauthier. 2017. Membrane tension controls adhesion positioning at the leading edge of cells. *The journal of cell biology.*

[12] Alexander Mogilner and George Oster. 1996. Cell Motility Driven by Actin Polymerization. *Biophysical Journal* Vol. 71, pp 3030-3045.

[13] Haguy Wolfenson Thomas Iskratsch and Michael P. Sheetz. 2014. Early Events in Cell Spreading as a Model for Quantitative Analysis of Biomechanical Events. *Biophysical journal* Vol. 107, pp 2508-2514.

[14] Thomas D. Pollard and John A. Cooper. 2009. Actin, a Central Player in Cell Shape and Movement. *American Association for the Advancement of Science*, Vol. 326, pp. 1208-1212.

[15] Dikla Raz-Ben Aroush, Noa Ofer, Enas Abu-Shah, Jun Allard, Oleg Krichevsky, Alex Mogilner, Kinneret Keren. 2017. Actin Turnover in Lamellipodial Fragments. *Current Biology* 27, pp 1-11, e1-e14.

[16] Kiran S. Kollepara, Paris D. Mulye, Pablo Saez. Fully Coupled Numerical Model of Actin Treadmilling in the Lamellipodium of the Cell. 2018. *International journal for numerical methods in biomedical engineering* Vol. 34, num. 12, pp. 1-21

[17] Alfio Quarteroni. 2008. Numerical Methods for Differential Problems. Volume 2. Ed. Springer.